ACS APPLIED MATERIALS & INTERFACES

NTNU

Subscriber access provided by NTNU University Library

Applications of Polymer, Composite, and Coating Materials

Fabrication and Evaluation of Bio-based Nanocomposite TFC Hollow Fiber Membranes for Enhanced CO2 capture

Zhongde Dai, Jing Deng, Qiang Yu, Ragne M Lilleby Helberg, Saravanan Janakiram, Luca Ansaloni, and Liyuan Deng

ACS Appl. Mater. Interfaces, **Just Accepted Manuscript** • DOI: 10.1021/acsami.8b19651 • Publication Date (Web): 22 Feb 2019

ACS Publications

is published by the American Chemical Society. 1155 Sixteenth Street N.W., Washington, DC 20036

Fabrication and Evaluation of Bio-based Nanocomposite TFC Hollow Fiber Membranes for Enhanced CO_2 Capture

*Zhongde Dai, Jing Deng, Qiang Yu, Ragne M. L. Helberg, Saravanan Janakiram, Luca Ansaloni, and Liyuan Deng**

Department of Chemical Engineering, Norwegian University of Science and Technology

Trondheim, 7491, Norway

KEYWORDS:

Nanocellulose; Nanocomposite; TFC membrane; Hollow fiber; CO_2 separation

ABSTRACT:

Nanocellulose is a promising and sustainable bio-based nanomaterial due to its excellent mechanical properties, biocompatibility, natural abundance, and especially its high aspect ratio. Interest in applying nanocellulose as nanofillers in membrane fabrication has been growing rapidly in recent years. In the present work, nanocellulose crystals (CNC) and nanocellulose fibers (CNF) were incorporated into polyvinyl alcohol (PVA) to prepare evenly dispersed nanocomposite. The resultant nanocomposite materials containing up to 80 wt% of nanocellulose were coated as defect-free, thin-film-composite (TFC) selective layers onto hollow fiber membrane substrates via dip-coating for efficient CO_2 capture. TGA, FTIR, XRD, STEM, SEM, and humid mixed gas permeation test were used to evaluate the nanocomposite materials and the membranes. The resultant PVA/CNC nanocomposite membranes exhibit both higher CO_2 permeance and CO_2/N_2 selectivity compared to the PVA/CNF membranes and the neat PVA membranes. The addition of CNC showed more positive effects on the CO_2 permeation compared to CNF. Under optimized conditions, CO_2 permeance of 672 GPU with a CO_2/N_2 selectivity of 43.6 was obtained with a PVA/CNC membrane. Excellent long-term stability of the membrane was also documented within a period of up to one year. The interface between the polymer phase and the charged nanocellulose fibers is believed to form fast gas transport channels at humid state and thus enhances CO_2 permeation.

1. Introduction

Cellulose is the most important natural polymer and a linear biopolymer consisting of glucan chains with repeating β-(1–4)-D-glucopyranose units, available in large quantities on earth.[1-2] In the recent decades, fundamental and applied studies of nanocelluloses, i.e., cellulose nanocrystals (CNCs, also referred to as nanocrystalline cellulose (NCC) or cellulose nanowhiskers (CNWs)), cellulose nanofibrils (CNFs, also referred to as nano-fibrillated cellulose (NFC)) and bacterial cellulose (BCs), have been rapidly expanding.[3-4] Cellulose nanoparticles are characterized by a high aspect ratio and low density. Surface modification of cellulose nanoparticles is easy due to the high density of reactive hydroxyl groups on its surface. CNCs are small (nanometric dimensions in both width and length), rod-shaped crystals consisting predominantly of crystalline cellulose, with very little amorphous cellulose, while CNFs contain both phases and are longer with a smaller diameter. Due to its renewable nature, excellent mechanical properties, good biocompatibility, broad chemical-modifying capacity and interesting optical properties, nanocellulose has been widely studied as potential materials in photonics, films and foams, thermoplastic materials, food packaging, and medical applications.[3, 5-7]

Recently, nanocellulose has been reported as additives in membranes for different separation applications. Karim et al.[8] employed CNCs as functional entity in chitosan for the removal of dyes from water in an ultrafiltration process. Nanocellulose has also been used as tight aqueous ultra-filtration membranes for different liquid purification processes.[9] For example, by using different kinds of nanocellulose (e.g., CNFs, CNCs, BCs, and TEMPO-oxidized CNFs) or functionalization strategies, the properties of the membranes, such as mechanical properties, porosity and pore size, can be accurately tuned.[9-11] The functionalized membranes have been used in hemodialysis[12], wastewater treatment[13], particle removal[10] and heavy metal ion removal[13]. Compared to the large

number of published papers applying nanocellulose in aqueous liquid separation/purification, using nanocellulose in gas separation membranes has rarely been reported [14]. Zhang et al.[15] used nanocellulose as polymeric matrix to hold Zn^{2+} ion as facilitated transport agents for CO_2 separation. Flexible and transparent membranes have been obtained with a CO_2 permeability of 155.0 Barrer, CO_2/N_2 selectivity of 27.2 and CO_2/O_2 selectivity of 100.6. Ansaloni et al.[16] investigated the CO_2 separation performances of microfibrillated cellulose (MFC) membranes at different relative humidity conditions, in which very good CO_2/N_2 and CO_2/CH_4 selectivity (in the order of 500 and 350, respectively) were obtained for neat MFC membranes. Mixing the MFCs with polyvinylamine (Lupamin®) could significantly improve the CO_2 permeability, but the selectivity is sacrificed. Similarly, Venturi et al.[17-18] mixed nanofibrillated cellulose (NFC) into Lupamin® and systematically investigated the different properties of the resulted nanocomposite membranes. It was found that the gas permeability increases linearly with the increase of RH value. However, the selectivity of the resultant membrane showed the optimum at RH around 60%. Under optimized condition, membranes with 30 wt% NFC and 70 wt% Lupamin showed the maximum selectivity values of 218 and 184 for CO_2/N_2 and CO_2/CH_4 gas pairs, respectively. Hosakun et al.[19] employed ATR-FTIR to study the interaction of CO_2 with bacterial cellulose-based (BC) membranes. It was reported that the hydroxyl groups from BC act as Lewis bases or electron donors that have strong interactions with the CO_2 molecules, which makes the BC also interesting materials for CO_2 separation.

Among the above mentioned reports on nanocellulose-based membranes in gas separation, most of the membranes were flat sheet self-standing membranes with a thickness of around 50 ~ 100 μm. Further work to develop thin-film-composite (TFC) membranes of the nanocellulose-based nanocomposite membranes are desired since in a membrane the gas permeance is inversely

proportional to the thickness of the dense selective layer. In practical applications, in order to reach a sufficient gas flux through membranes and thus making the separation process economically feasible, membranes with a defect-free selective layer thickness ranging from 0.1 to 1.0 μm are usually required[20]. Applying nanocellulose in thin-film-composite (TFC) membranes has been rarely reported except for a few reports from our prior works, [21-22] in which the nanocellulose contents in the membranes were in a much lower range (< 4 wt%) [22] and the CO_2 permeance (< 100 GPU) was considered not practical for industrial applications. In addition, the membranes were fabricated only as flat sheet. For post-combustion CO_2 capture, however, hollow fiber membrane modules are more efficient to treat the huge amount of the flue gas [20, 23].

In the present study, CNCs and CNFs were blended with polyvinyl alcohol (PVA) to fabricate nanocellulose-based nanocomposite TFC hollow fiber membranes with a sub-μm coating layer. Poly(p-phenylene oxide) (PPO) hollow fibers were used as the supporting substrate. Compared to the flat sheet membranes, hollow fiber membranes have several distinct advantages for gas separation, such as self-supporting characteristic, high surface-to-volume ratio and easiness of up-scaling [20, 23]. The nanocellulose content in the membranes was increased up to 80 wt%, which demonstrated the possibility of using a sustainable biopolymer to partly replace the conventional synthetic polymeric membrane materials produced from petroleum industry. PVA was selected as the polymer matrix because of its excellent film-forming properties, mechanical strength as well as its non-toxic and biodegradable features. Moreover, the PVA based membranes have been well-studied and the desired properties been confirmed in our prior works.[24-25] The PVA/nanocellulose nanocomposite selective layers were coated on the PPO support via a dip-coating method, which is a simple but effective approach, allowing easy control of the thickness and up-scaling. The thermal, chemical and morphological properties of the synthesized membranes were characterized

using TGA, SEM, FTIR, and XRD. The gas separation performances of the resultant TFC hollow fiber nanocomposite membranes were evaluated by humid mixed gas permeation test. Long-term stability test of the hollow fiber membrane module was carried out in a period of one year.

2. Experimental

2.1. Materials

PPO hollow fiber membrane (inside diameter ~350 μm, outside diameter ~540 μm) was supplied by Parker Hannifin A/S, Norway. Polyvinyl alcohol (PVA, Mn=7.9k ~ 12k, 89% hydrolyzed) was purchased from Sigma, Norway. Nanocellulose crystal (CNC, sulfuric acid process, aqueous slurry with a concentration of 12.1 wt%) made from wood pulp was ordered from the University of Maine, USA. Nanocellulose fibers (CNF, water dispersion with a concentration of 3 wt%) was kindly provided by Inofib, France. All chemicals were used without further purification.

2.2 Membrane and membrane module preparation

PVA was firstly dissolved in water at 80 °C for 4 hours under reflux to make 2 wt% solution. The desired amount of CNC or CNF was mixed with the PVA solution at room temperature (the temperature range of 22 to 25 °C in this work). The total solid concentration was adjusted to 0.5 wt% in water. The PVA/nanocellulose mixture was stirred for at least 6 hours before dip-coating.

The nanocellulose content (ω_{NC}, wt%) in each membrane was calculated from Eq. (1):

$$\omega_{NC} = \frac{w_{NC}}{w_{NC} + w_{PVA}} \times 100 \quad (1)$$

where w_{NC} and w_{PVA} are the mass of nanocellulose and PVA, respectively.

The TFC hollow fiber membranes were prepared via a dip-coating method [26] with commercial PPO hollow fiber membranes as the support substrate. It is worth mentioning that the PPO hollow fiber membranes have a thin dense layer with the CO_2 permeance of around 3000 GPU and a CO_2/N_2 selectivity of around 17 at the dry state, which are in good agreement with literature values [27]. The PPO hollow fibers were washed with DI water and dried at room temperature for ~ 30 minutes before the dip-coating step. The fibers were then dipped into the PVA/nanocellulose aqueous solutions for 5 seconds and withdrew steadily. After drying at room temperature for at least 4 hours, the second coating was applied with the same coating procedure, turning the membrane upside down to achieve a uniform coating layer. After the solvent was evaporated at room temperature, the membrane was moved into a vacuum oven for at least 6 h at 60 °C before the fabrication of the membrane module.

PVA/nanocellulose self-standing films with the same composition of the thin coatings were prepared for TGA, XRD, and FTIR characterizations. The PVA/nanocellulose suspensions were poured into a Teflon petri dish and dried at 50 °C overnight in a convective oven to make the self-standing films.

2.3 Characterization

The dimensions of the nanocellulose were measured by a transmission electron microscope (TEM). Around 0.5 g of the nanocellulose suspension was diluted in 50 ml acetone and sonicated for 4 mins. then a 300-mesh copper grid was placed on a filter paper, a few drops of the acetone solution was added onto the mesh. After the mesh was dried in ambient condition, it was analyzed using a JEM-2010 electron microscope (Jeol, Japan).

The rheological properties of the PVA/nanocellulose suspensions was measured at 25 °C with a Waters HR-2 Discovery Hybrid Rheometer (TA instrument) using a cone-plate configuration (40 mm parallel plate, Peltier plate Steel). The steady state shear viscosity was measured at shear rates between 1 and 200 s^{-1}. For each sample, at least two tests were carried out and the error was found to be always lower than 10%.

The thermal stability of the PVA/nanocellulose nanocomposites was investigated via thermal gravimetric analysis (TGA) by a thermo-microbalance from Netzsch (TG 209F1 Libra). Samples of around 10 mg were used. The test temperature was ranging from ambient temperature to 700 °C. N_2 gas was used as both protective flow and sweep flow during the TGA test.

The crystallinity of the PVA/nanocellulose nanocomposites was characterized using a Bruker D8 A25 DaVinci X-ray Diffractometer with Cu Kα radiation of characteristic wavelength λ=1.54 Å. The scans were taken in the 2θ range with a step size 0.01° from 5° to 75°.

The membrane morphology was studied using a scanning electron microscope (SEM, TM3030 tabletop microscope, Hitachi High Technologies America, Inc.). Surface samples were prepared using scissors and cross-section specimens were prepared by breaking the samples in liquid N_2. All the samples were sputter coated with gold for 2 minutes to ensure good electrical conductivity.

Fourier-transform infrared (FTIR) spectroscopy was performed using a Thermo Nicolet Nexus spectrometer with a smart endurance reflection cell. Spectrums were averaged over 16 scans at a wavenumber resolution of 4 cm^{-1} in the range of 650 cm^{-1} to 4000 cm^{-1}.

Gas-separation performance was tested in the mixed-gas setup, as schematically depicted in **Figure 1**. Details of the experimental setup are reported elsewhere.[28-29] A CO_2/N_2 gas mixture

(10%/90% vol) constituted the feed gas, whereas pure CH_4 was used as the sweep gas instead of Helium since Helium was used as the carrier gas for the gas chromatograph (GC). For all the experiments, the feed pressures were held constant at 2.0 bar while the sweep side pressure was kept at 1.05 bar. In the present study, all the gas permeation tests were carried out under fully-humidified conditions (100% RH). The compositions of retentate and permeate streams exiting the membrane module were monitored by a calibrated gas chromatograph (490 Micro GC, Agilent) over the duration of the test. Each test lasted for at least 6 h to ensure the observation of the steady state of permeation.

The permeance (P_i) of the *i*th penetrant species can be calculated from Eq.(2):

$$P_i = \frac{N_{perm}(1 - y_{H2O})y_i}{A(p_{i,feed} - p_{i,perm})} \quad (2)$$

where N_{perm} is the total permeate flow measured with a bubble flow meter (ml/min), y_{H_2O} is the molar fraction of water in the permeate flow (calculated according to the RH value and the vapor pressure at the given temperature), y_i is the molar fraction of the species of interest in the permeate flow (%), and $p_{i,feed}$and $p_{i,perm}$ identify the partial pressures of the *i*th species in the feed and permeate, respectively. In the present work, the gas permeance is expresses in the unit of GPU (1 GPU = 10^{-6} cm^3 (STP) cm^{-2} s^{-1} (cm Hg)$^{-1}$). Both feed flow and permeate flow were kept rather high to ensure low stage cut and constant driving force along the membrane module. The separation factor ($\alpha_{i/j} = \frac{y_i/x_i}{y_j/x_j}$) was applied for mixed-gas permeation tests. The ideal selectivity ($\alpha^i_{A/B} = \frac{P_{m,A}}{P_{m,B}}$) was also determined here, variation between ideal selectivity and separation factor was less than 5% (due to the low stage-cut), thus only the separation factor was reported in the

current study.

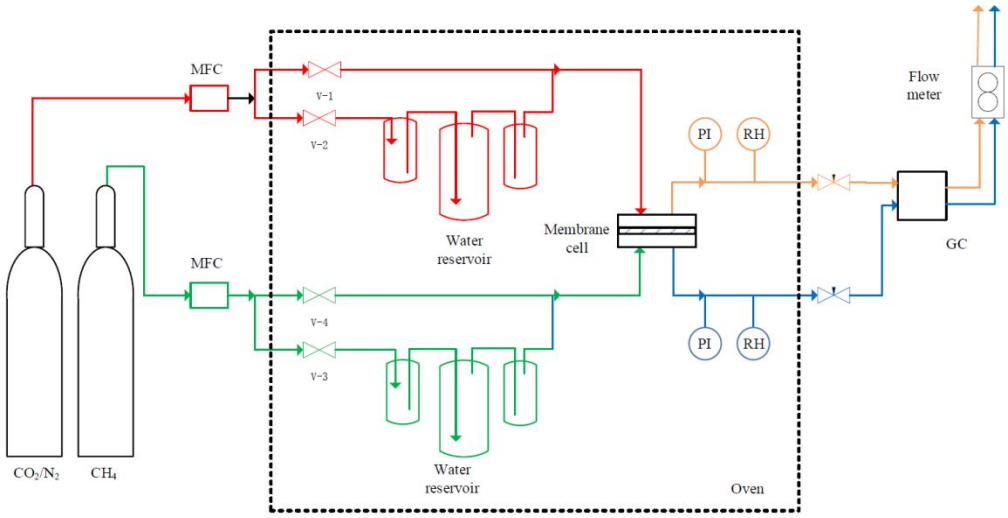

Figure 1. Mixed-gas permeation setup. MFC--- mass flow controller, PI---Pressure indicator, RH---relative humidity sensor. GC---gas chromatograph.

3. Results and Discussion

3.1 Nanocellulose morphology study

CNCs are typically prepared by strong acid (e.g., H_2SO_4) hydrolysis of the cellulose pulp, allowing dissolution of the amorphous regions of the cellulose polymer.[30] Acid resistant crystals with negatively charged sulfate groups at the surfaces are the main product of this process. Production of CNF can generally be divided into the following steps: 1) pretreatment of cellulose pulp to facilitate fiber separation/delamination (e.g. mechanical cutting, acid hydrolysis, the introduction of charged groups), and 2) mechanical step to further reduce the size of fibers to nm-dimensions (e.g. homogenizing, grinding). It is well-accepted that the raw material is the most important factor

influencing the nanocellulose's dimensions as well as its hydrolysis conditions and/or pretreatments. For instance, the morphology and aspect ratio (length/diameter) of the nanocellulose extracted from different biomass sources can be significantly different. Therefore, the CNC and CNF used in this work were studied in a TEM to investigate the morphology of these two additives in the membranes.

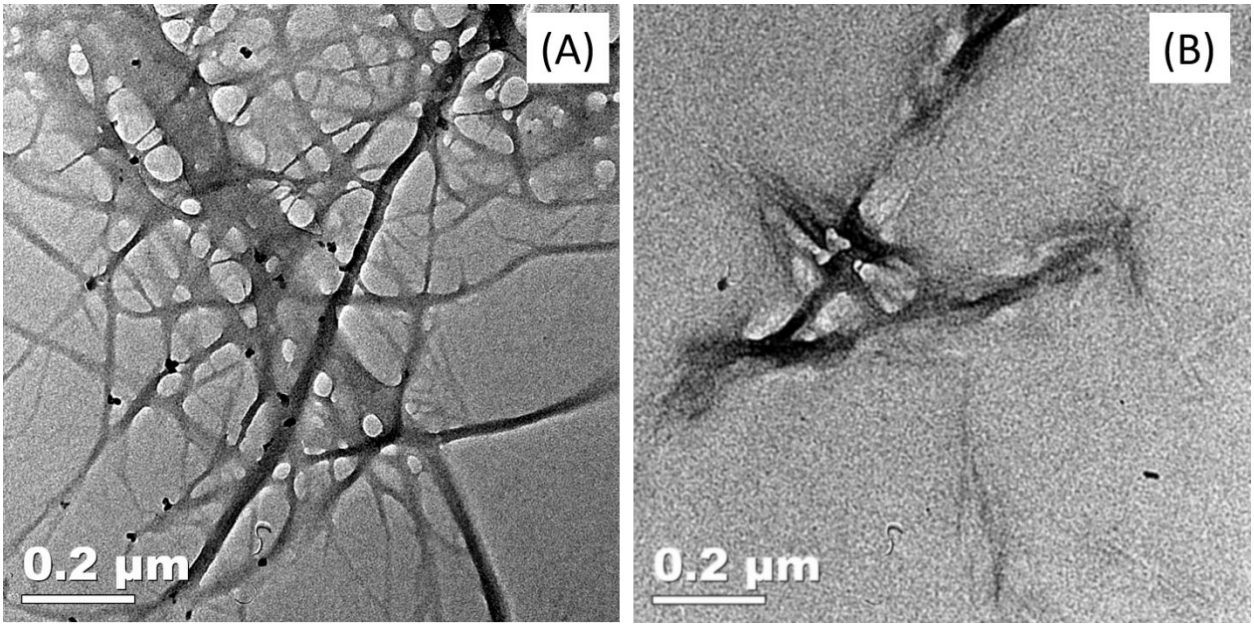

Figure 2. TEM image of the CNF (A) and CNC (B).

According to the TEM images, CNFs show a length of hundreds of nanometers (**Figure 2A**) similar to previous observations from the literature[31]. In addition, it is clearly depicting agglomeration of CNF fibers in the suspension even when the concentration is as low as 0.5 wt%. According to the supplier, the CNFs used in this work have a high tendency of forming aggregates, thus only mild magnetic stirring was used to disperse the CNFs in water. In the case of the CNC, **Figure 2B** shows a typical CNC morphology as reported in the literatures[2, 32]. The CNCs are

relatively bigger compared to the CNF fibers, but with relatively shorter length, which is in good agreement with literature values. Furthermore, a small amount of granular substances was observed in both CNF and CNC samples. Most likely, these particles are residual lignin fragments produced in the CNC production process [33].

3.2 Thermal properties

Figure 3 presents the TGA curves of PVA/CNC and PVA/CNF nanocomposite materials. As it can be seen, adding CNFs into the PVA matrix does not significantly influence the thermal stability. A T_{onset} of ~280 °C can be found for the neat PVA membrane, while the difference between the T_{onset} of the nanocomposite membrane and that of the neat PVA is negligible. T_{onset} is the intersection of the baseline weight and the tangent of the weight dependence on the temperature curve as decomposition occurs. The T_{onset} value of PVA obtained from this work is comparable with literature data (287 °C). [34] It is commonly accepted that the thermal properties of PVA may change with its molecular weight as well as with the hydrolysis degree. In the present study, a small weight loss could be found for almost all the PVA samples in the temperature range of 80 ~ 150 °C, possibly due to the small amount of residual water in the membrane sample.[34] In addition, it is observed that as the nanocellulose content increases, the weight loss reduces, probably due to less water remained in the CNC and CNF than in the neat PVA.[16, 35] On the other hand, a higher residual content can be found for the CNF material, which is around 30% at 700 °C, possibly due to the fact that the cellulose chains could form more stable crosslinking network at high temperatures and the decomposition is thus not completed.[36] In addition, the mass residual of the PVA/CNF membranes is proportional to the CNF content in the membrane. The PVA sample completely decomposed at temperatures higher than 600 °C.

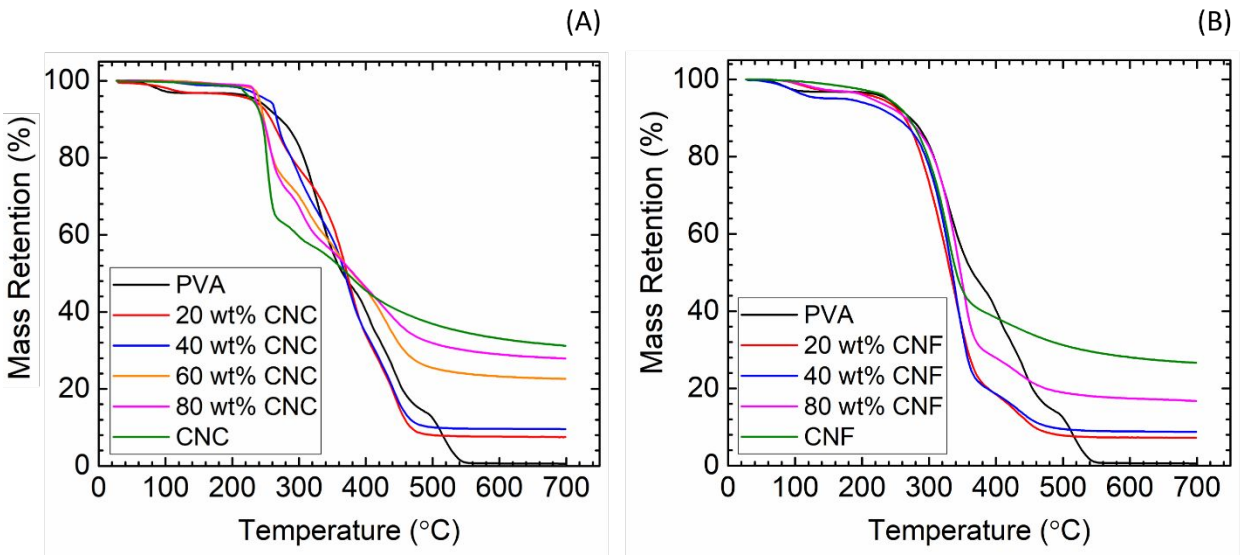

Figure 3. TGA of PVA/CNC and PVA/CNF nanocomposite membranes.

Adding CNC into PVA matrix has also a very limited effect on the first stage decomposition: a T_{onset} of around 280 °C was found for all the samples. Compared to the neat PVA or CNF samples, the CNC sample has a deep decomposition curve at around 250 °C, indicating a sharp thermal decomposition/reaction.[37] Similar to the CNF samples, the CNC samples have also a higher residual mass compared to the PVA sample, possibly due to the formation of more thermally stable cross-linked structure from the CNC fibers. The residual mass is proportional to the CNC content in the nanocomposite membranes as well.

3.3 FTIR analysis

The FTIR spectra of the PVA/CNC and PVA/CNF nanocomposite membrane materials are shown in **Figure 4**. Detailed peak assignments are listed in **Table 1**.

Table 1. FTIR peak assignments, reproduced with permission from ref [38]

Wavenumber (cm^{-1})	Peak assignment
3350	O-H stretching
2900	C-H_n stretching
1730	C=O of ketone
1630	Absorbed water
1430	CH_2 bending
1370	C-H deformation
1320	CH_2 deformation
1244	C-O stretching of the ether linkage
1201	OH in-plane bending
1051	C-O symmetric stretching of primary alcohol
1037	C-O stretching
898	β-glucosidic linkages between the sugar units

The abundant presence of hydroxyl groups on both PVA and nanocellulose determines the broad peak at the wavelength of 3000 ~ 3500 cm^{-1} for all the samples. The intensity appears to be independent of the content of the CNC or CNF in the PVA matrix. In addition, as the PVA used in this study has a hydrolysis degree of 87 ~ 89%, about 11 ~ 13% of acetate groups are still present in the polymer phase, generating the C=O peak located at 1730 cm^{-1}.[39] It is also found that the peak at 2900 cm^{-1} is much stronger for the PVA sample and it reduces with increasing the CNC/CNF content, which can be explained by the relatively higher C/H ratio in PVA sample than the CNC/CNF samples. The peak located at 1630 cm^{-1} is attributed to the bending of free water molecules and, clearly, the addition of nanocellulose (both CNCs and CNFs) reduced the peak intensity, indicating a lower water residual upon sample preparation. This is consistent with the different water uptake features shown by nanocellulose and PVA[16, 35] and with the TGA results as reported in **Figure. 3**.

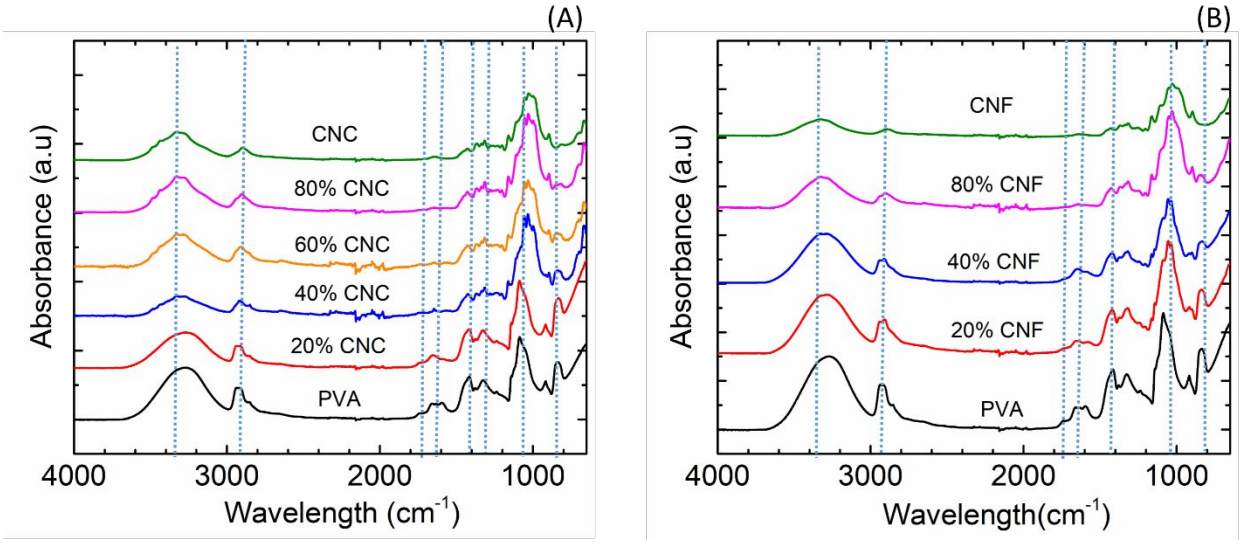

Figure 4. FTIR of PVA/CNC and PVA/CNF nanocomposite membrane with various additive content.

3.4 XRD analysis

XRD was applied to characterize the crystallization properties of the PVA/nanocellulose nanocomposite membranes. The XRD patterns of the PVA/nanocellulose nanocomposite are shown in **Figure 5** and characteristic XRD peaks of CNC and PVA are listed in **Table 2.** It is commonly accepted that dry CNCs include two polymorphs: cellulose I and II.[40-41] Cellullose I is the native crystalline phase formed mainly due to hydrogen bonding, in which the cellulose chains form sheets connected with each other. Cellulose II is considered as the "man-made" form of cellulose, which is generally formed in the process of dissolving/regenerating the cellulose, or swelling cellulose in concentrated alkali solution. The detailed peak assignments can be found in **Table 2**.

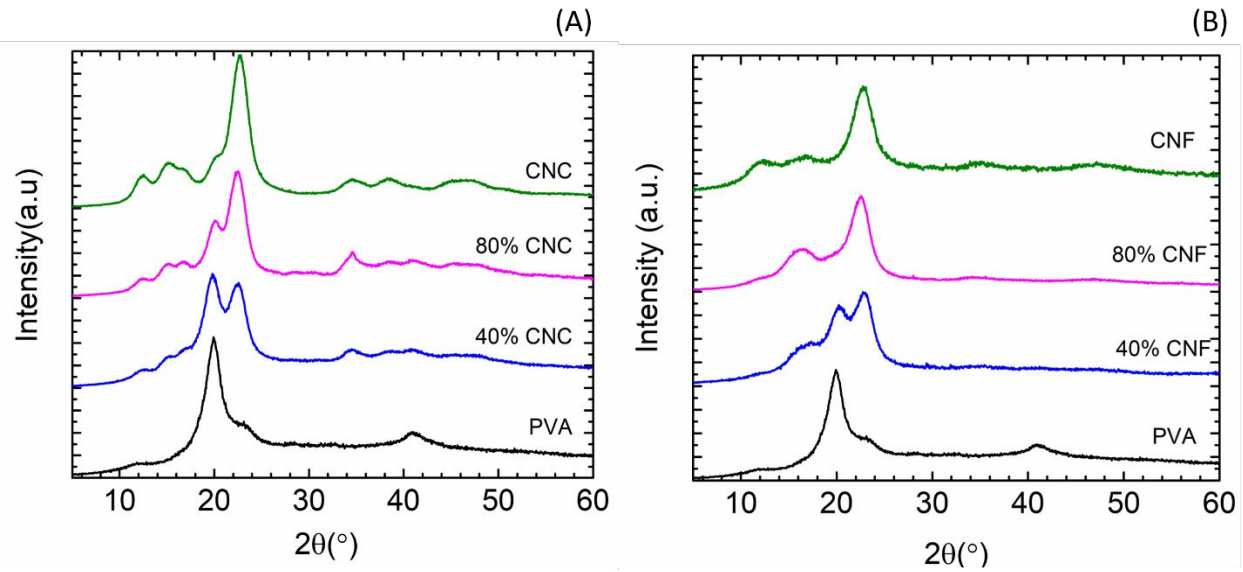

Figure 5. XRD pattern of PVA/CNC (A) and PVA/CNF (B) nanocomposite membrane with various additive content.

As can be found from both **Figure 5** and **Table 2**, the characteristic peaks of CNC are in good agreement with the literature.[36] It is worth mentioning that for CNF samples, the XRD peaks are the composite peaks of diffraction intensity of the assigned crystalline plane with several other crystalline planes.[42] It is also possible that the overlapping of the diffraction signals of these crystalline planes broadened the width of the obtained diffraction peaks.

Table 2. Characteristic XRD peak of CNC and PVA

	Peak position (°)	Miller indices
CNC	12.1	−110 for cellulose II
	19.8	110 for cellulose II
	14.9	−110 from cellulose I
	16.4	110 from cellulose I
	22.6	200 for both celluloses I and II
	34.5	004 for both celluloses I and II
CNF	14.8	-110
	16.3	110
	22.6	200
	34.5	004
PVA	19.4	101
	40.4	--

The crystallinity of the different nanocellulose samples was estimated by using the "Segal's method", a commonly used method for the calculation of crystallinity index (CI) of cellulose.[43] According to this method[44], the crystallinity index can be calculated by Eq. (3):

$$X_C = 100 * \frac{I_{200} - I_{AM}}{I_{200}} \quad (3)$$

Where the X_C is the crystallinity index and the I_{200} is the 200 peak. In our study, the highest peak represents both crystalline and amorphous material. I_{AM} is the lowest height between 200 peak and 110 peak, which represents only the amorphous part. Based on Segal's method, the crystallinity index of CNFs in our study is calculated to be 69.2%, which is slightly lower than the reported value (between 73 ~ 82%).[42] However, it is noteworthy that the processing/drying process have a significant impact on the crystallinity of the nanocellulose. Even if starting from the same nanocellulose suspension, different processing/drying procedure may result in big deviations in XRD results. [36] Considering the CNC samples, two 110 peaks can be found from the XRD patterns of CNC (as shown in **Table 2**), so the calculation of the relative crystallinity is non-trivial. However, as reported in literature[45], if the I_{AM} at 18.2° is considered, then the crystallinity index of the CNC can be calculated as 82.9%. As expected, the CNC shows relatively higher crystallinity index value than the CNF.

PVA is a semi-crystalline polymer. The curve shown in **Figure 5** indicates that PVA had significant diffraction peaks at 2θ = 11.4, 19.4 and 40.4°. Specifically, the sharp peak at 19.6° is the main crystal peak, corresponding to a (101) reflection of the monoclinic crystal.[46] The high degree of crystallinity of PVA can be attributed to the regularity in the molecular structure.[47] For both PVA/CNC and PVA/CNF nanocomposite materials, the big peak at 22.6° reduces as the

content of CNC/CNF decreases. On the other hand, the peak at 19.4°, corresponding to PVA, increases along with the PVA content. At a lower CNC/CNF content, some of the nanocellulose peaks overlapped with the PVA peaks. Adding CNC/CNF into PVA matrix does not change the peak position or peak shape, indicating that there is no significant chemical interaction between the PVA and CNC/CNF.[38]

3.5 Membrane morphology study

SEM has been used to investigate the morphology of the hollow fibers membranes used in the present study and the results are shown in **Figure 6**. In the case of the neat PPO substrate, an asymmetric structure with a dense skin layer at the outer side of the hollow fiber can be observed, as presented in **Figure 6 (A)**. Compared to the SEM image of neat PPO, from **Figure 6 (B)** it can be seen that an ultrathin PVA layer has been successfully coated onto the PPO substrate. The outer skin layer of the asymmetric hollow fiber is critical to prevent the penetration of the coating solution into the pores of the fibers. From **Figure 6 (C)-(F),** the SEM images of the PVA/CNC and PVA/CNF membranes containing different amount of CNCs and CNFs, it can be seen that the addition of CNCs and CNFs has different effects on the thicknesses of the coating layers. For PVA/CNC nanocomposite membranes, the increase of CNCs content in the PVA matrix showed a limited influence on the thickness of the coating, whereas, in the case of the PVA/CNF nanocomposites, the addition of CNFs in the coating material has led to a notable increase of selective layer thickness. The surface morphology of the various membranes is shown in the insets in **Figure 6**. For the neat PVA and PVA/CNC membranes, homogeneous surfaces were obtained for all blend compositions. In the case of PVA/CNF membranes, however, aggregation spots were observed on the surfaces, possibly due to the poor dispersion of the CNF fibers in a suspension with relatively high viscosity. Increasing the stirring time from 6 hours to 2 days did not

significantly improve the CNF dispersion, but sonication was not used in this work since according to the supplier, the CNF fibers have a high tendency of forming connected structures under sonication.

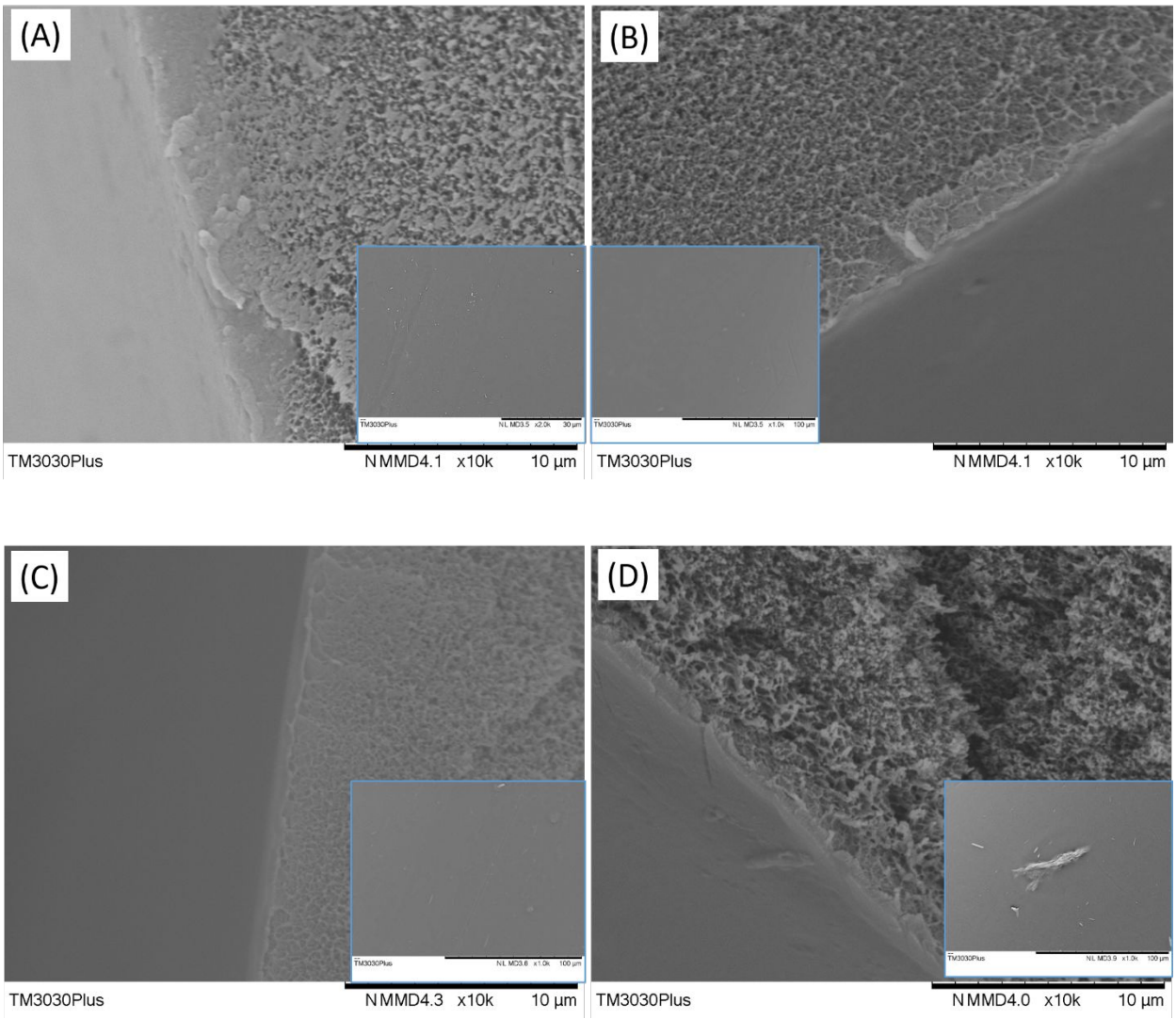

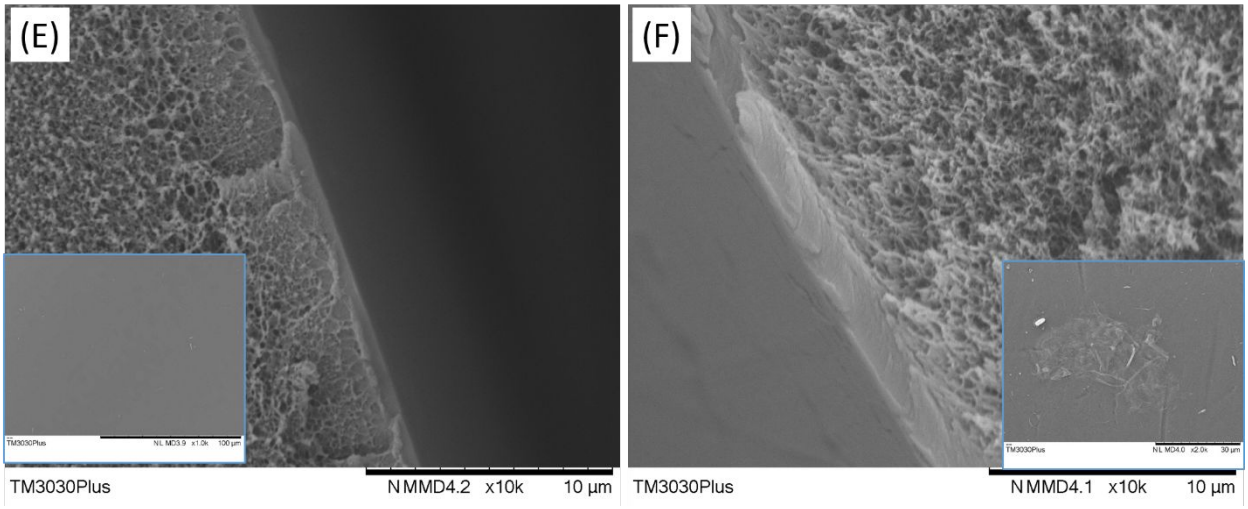

Figure 6. Morphology of PVA/CNC and PVA/CNF nanocomposite membrane coated on PPO hollow fiber support, the inset figures are the membrane surface images. (A) PPO, (B) PPO-PVA, (C) PPO-20%CNC, (D) PPO-20%CNF, (E) PPO-80% CNC, (F) PPO-80%CNF.

The numerical values of the selective layer thickness for the different blending compositions are presented in **Figure 7A.** As shown in the figure, the coating thickness increases along with the nanocellulose content but to a different extent, depending on the nanocellulose type. Increasing the CNF content in PVA resulted in a significant thickening of the selective layer, while a minor variation could be observed for the CNCs blend, which appeared independent of the nanocellulose content. An explanation of the observed behavior can be found by analyzing the viscosity of the PVA/CNC and PVA/CNF coating solutions, where the total solid content was maintained at 0.5 wt%. As shown in **Figure 7B**, the addition of CNCs into the PVA solution makes a negligible effect on the overall viscosity of the coating solution. At a higher CNCs content, the viscosity of the suspension approaches that of the neat CNC suspension with 0.5 wt% solid content (1.14 mPa·s), which is slightly lower compared to that of the neat PVA solution (1.37 mPa·s). Contrarily, adding CNFs into PVA solution leads to significant increase in viscosity, from 1.4 to 6.3 mPa·s.

The viscosity trends correlate in a suitable manner with those of the selective layer thickness, clearly suggesting that the higher viscosity in the PVA/CNF coating solution at the same nanocellulose content compared with that of the PVA/CNC coating solution is probably the main reason for the thicker PVA/CNF coating layers.

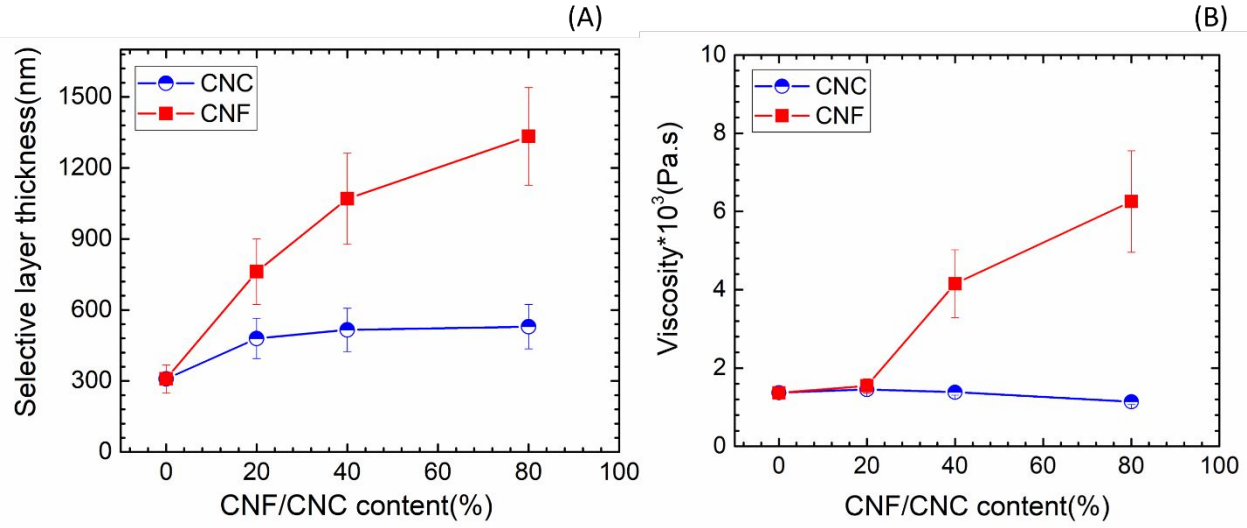

Figure 7. Viscosity of the coating solution (constant solid content = 0.5 wt%) (A) and resultant membrane selective layer thickness (B) with different CNCs or CNFs amounts.

3.6 Mixed-gas permeation tests

The gas permeation properties of the PVA/CNC and PVA/CNF nanocomposite membranes were investigated using CO_2/N_2 (10%/90% vol) mixture as feed gas under fully humidified (~ 100% RH) conditions. The separation performances of the membranes are presented in **Figure 8**.

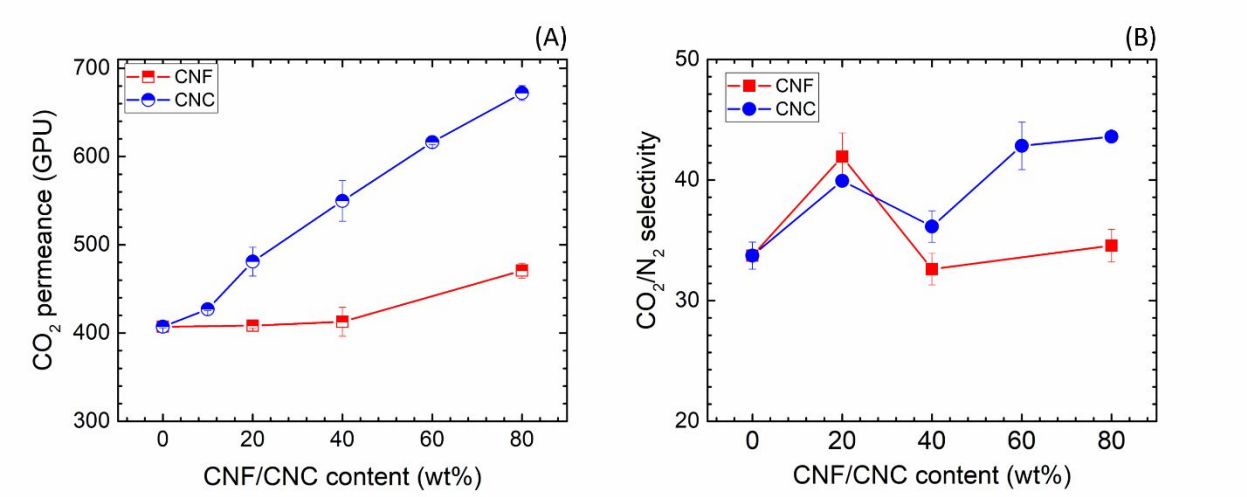

Figure 8. CO_2 permeance (A) and CO_2/N_2 selectivity (B) of the PVA/nanocellulose nanocomposite membranes as a function of nanocellulose content. Tested at R.T. using fully humid feed gas.

As presented in **Figure 8A**, adding both CNFs and CNCs into PVA matrix of the membranes leads to an increase in the CO_2 permeance. However, it is evident that the addition of CNCs in a PVA-based membrane is much more effective in enhancing CO_2 permeance compared to CNFs; Starting from the neat PVA membrane, the CO_2 permeance increases from 407 GPU to 672 GPU by adding up to 80% CNC, corresponding to a 65% enhancement. On the other hand, the improvement in CO_2 permeance by the addition of CNFs in the membranes is scanty; At a CNF content lower than 40 wt%, the CO_2 permeance through the composite membranes remained nearly unchanged (from 407 GPU to 413 GPU), and it increased to 471 GPU at 80 wt% CNF, resulting in only a 15% enhancement. The significantly increased CO_2 permeance in the PVA/CNC membranes may be mainly attributed to the enhancement of the specifically located water swelling resulted from the increased chain twists/nano-spaces, which are created by the presence of the nano-size rod-shaped CNCs. This kind of nano-space may also serve as water reservoirs to keep the water uptake upon the fluctuation of the humidity in the feed and keep the membrane at the optimal water swelling

conditions for CO_2 transport. Similar nano-spacer effect has been reported by Deng et al in a membrane with CNTs as nanofillers. [48] In addition, the hydrophilic outer surface of the CNCs may have also created water rich channels at the interface with the PVA matrix, which accelerates the gas transport as well, especially the transport of CO_2, the more reactive gas with water. It is reported that the water uptake of the nanocellulose appears lower than that of the PVA polymer[25, 49], thus adding nanocellulose into PVA matrix probably reduces the overall value of the swelling degree of the blends. However, nanocellulose is characterized of a higher CO_2-philicity compared to PVA and the swelling of the nanocellulose at the outer surface at high RH value could create a path along the nanocellulose that favors the CO_2 transport.[50]

In the PVA/CNF membranes, however, instead of creating additional nano-spaces for water, the entanglement of the long CNF fibers may form contextures that constrain the swelling of the PVA matrix, thus the effects of CNF to the enhancement of gas permeation is limited and the CO_2 permeance of the PVA/CNF membranes are much lower compared to the PVA/CNC membranes. Another reason for the lower CO_2 permeances of the PVA/CNF membranes is due to the thicker selective layers in the TFC membranes; The presence of CNFs in PVA solution results in the increase of the viscosity of the coating solutions, and thus a much thicker coating at a similar nanocellulose content.

The effects of nanocelluslose content on CO_2/N_2 selectivity are reported in **Figure 8B**. As it can be seen, adding nanocellulose into PVA matrix in the TFC hollow fiber membranes leads to a moderate improvement on the CO_2/N_2 selectivity and the effects of CNC and CNF to the selectivity are also different**.** Neat PVA membrane exhibits a CO_2/N_2 selectivity of approximately 35 and adding CNCs into PVA matrix gradually increases the selectivity to about 45. The enhanced CO_2/N_2 selectivity with the addition of CNC is believed due to the formation of the CO_2

hydrophilic gas transport paths (the water rich channels) along the CNC outer surface under fully humid conditions as well. The only exception was found from the sample containing 40 wt% CNC. This exception was experimentally confirmed by multiple repetitions, and it is believed that the low CO_2/N_2 selectivity at 40 wt % CNC addition is related to the instability of the PVA/CNC solution at around this composition, since white flocculation was observed in the suspension shortly after it was prepared. At a lower CNCs content, the PVA phase in the suspension dominates and the long chains of the polymer are able to prevent the formation of CNCs aggregates. At a higher CNCs concentration, the CNC phase becomes dominating and the PVA chains disperse homogeneously within the CNC suspension; both cases lead to a relatively stable matrix. However, when the CNC content is around 40 wt%, there may exist a transition state, where CNCs start to aggregate and the suspension becomes unstable, forming flocculation and thus resulting in the uneven distribution of the CNCs in the membranes.

The change of the CO_2/N_2 selectivity with the nanoclellulose content has a different trend in the PVA/CNF membranes. At a low CNF content (e.g., < 20 wt%), the CO_2/N_2 selectivity of the PVA/CNF membranes increase with the increasing CNF content as well, which is similar to that of the PVA/CNC membranes and the improvement in selectivity is believed also due to the formation of the more CO_2-philic path along the surface of the added CNF fibers. However, further increase of the CNF content may result in the formation of the entanglement of the long CNF fibers that suppresses the swelling and hence the formation of the water rich channel along the fibers. The selectivity is thus decreases with the increasing CNF content until it reaches a value similar to that of the neat PVA membrane.

The stability of a membrane is of crucial importance for industrial applications. Generally, separation performance of polymeric membranes changes over time due to unavoidable aging. It

is reported that even the best membranes currently available on the market exhibit a decline of up to 30% in permeance in the first six months of operation.[20] In the present study, the PVA/CNC TFC membrane containing 80 wt% CNCs was selected to study the membrane stability because of its promising separation performance regarding both CO_2 permeance and CO_2/N_2 selectivity. The CO_2 separation performance of the membrane with time is shown in **Figure 9**. As it can be seen, the CO_2 permeance increases sharply in the beginning of the test and gradually stabilizes, reaching a plateau and staying stabilized for more than 40 hours. The gas permeation test was then shut down and the membrane was removed out from the gas permeation test rig and stored in humid air. Two weeks later the membrane was re-installed in the same system and tested again under the same conditions. The CO_2 permeation data obtained from the second round test were found comparable to the value from the first round test (CO_2 permeance in the range of 670 ~ 680 GPU and CO_2/N_2 selectivity of around 45); No significant decline of either CO_2 permeance or CO_2/N_2 selectivity was observed. After the second test, the membrane was kept in ambient condition for one year. The dry membrane was conditioned and tested again for the third time. As shown in **Figure 9**, the membrane shows no evident decline in either CO_2 permenace or CO_2/N_2 selectivity, demonstrating an excellent long time stability and practical handling of the membranes.

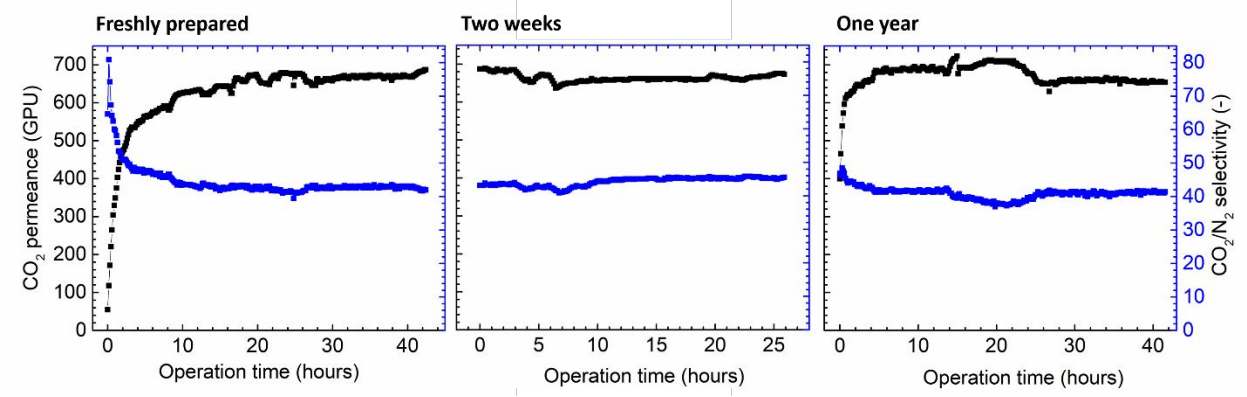

Figure 9. Long-term stability of separation performance of the PVA/CNC nanocomposite membranes (80 wt% CNCs) within one year.

4. Conclusion

In this work, two types of nanocellulose, CNC and CNF, were found to be effective nanofillers in nanocomposite membrane fabrication using PVA as polymer matrix. A defect-free nanocomposite selective layer was successfully coated onto a PPO hollow fiber substrate. PVA/CNC membranes exhibited higher CO_2 permeance and CO_2/N_2 selectivity compared to the PVA/CNF membranes. The different CO_2 permeation properties appeared in the PVA/CNC and PVA/CNF membranes and at different nanocellulose contents may be attributed to the different interaction of the PVA matrix and the different types of nanocellulose, and the different dispersion of CNC and CNF in the PVA matrix in the nanocomposite. The presence of CNFs in PVA solution increased the viscosity of the coating solutions, resulting in a much thicker selective layer, and thus the CO_2 permeance of PVA/CNF membranes are much lower than that of the PVA/CNC membranes with similar nanocellulose content. These nanocomposite membranes also showed excellent stability in separation performances and a long shelf time.

The separation performance of the membranes developed in the current work is in the range of industrial interests, and the materials used are sustainable, low cost and easy to process. This work may open a new window for the utilization of bio-based materials from nature for the fabrication of CO_2 separation membranes.

ASSOCIATED CONTENT

AUTHOR INFORMATION

Corresponding Author

* Liyuan Deng.

E-mail: deng@nt.ntnu.no, Tel.: +47 73594112,

ORCID:

Zhongde Dai: 0000-0002-3558-5403

Jing Deng: 0000-0003-3680-3799

Luca Ansaloni: 0000-0002-4930-0253

Liyuan Deng: 0000-0003-4785-4620

Author Contributions

The manuscript was written through contributions of all authors. All authors have given approval to the final version of the manuscript.

Notes

The authors declare no competing financial interest.

Funding Sources

This work was financially supported by the European Union's Horizon 2020 Research and Innovation program under Grant Agreement No. 727734 and from the CLIMIT program by the Research Council of Norway (No. 239172).

ACKNOWLEDGMENT

Dr. Dingding Ren (Department of Electronic Systems, NTNU) and Dr. Yingda Yu (Department of Materials Science and Engineering, NTNU) are highly acknowledged for the kind help in the TEM characterization.

REFERENCES

(1) Oksman, K.; Aitomäki, Y.; Mathew, A. P.; Siqueira, G.; Zhou, Q.; Butylina, S.; Tanpichai, S.; Zhou, X.; Hooshmand, S. Review of the Recent Developments in Cellulose Nanocomposite Processing. *Composites Part A* **2016,** *83*, 2-18, DOI: https://doi.org/10.1016/j.compositesa.2015.10.041.
(2) Sacui, I. A.; Nieuwendaal, R. C.; Burnett, D. J.; Stranick, S. J.; Jorfi, M.; Weder, C.; Foster, E. J.; Olsson, R. T.; Gilman, J. W. Comparison of the Properties of Cellulose Nanocrystals and Cellulose Nanofibrils Isolated from Bacteria, Tunicate, and Wood Processed Using Acid, Enzymatic, Mechanical, and Oxidative Methods. *ACS Appl. Mater. Interfaces* **2014,** *6* (9), 6127-6138, DOI: 10.1021/am500359f.
(3) Abitbol, T.; Rivkin, A.; Cao, Y.; Nevo, Y.; Abraham, E.; Ben-Shalom, T.; Lapidot, S.; Shoseyov, O. Nanocellulose, a Tiny Fiber with Huge Applications. *Curr. Opin. Biotechnol.* **2016,** *39*, 76-88, DOI: https://doi.org/10.1016/j.copbio.2016.01.002.
(4) Li, Q.; McGinnis, S.; Sydnor, C.; Wong, A.; Renneckar, S. Nanocellulose Life Cycle Assessment. *ACS Sustainable Chem. Eng.* **2013,** *1* (8), 919-928, DOI: 10.1021/sc4000225.
(5) Azeredo, H. M. C.; Rosa, M. F.; Mattoso, L. H. C. Nanocellulose in Bio-Based Food Packaging Applications. *Ind. Crop. Prod.* **2017,** *97*, 664-671, DOI: https://doi.org/10.1016/j.indcrop.2016.03.013.

(6) Klemm, D.; Schumann, D.; Kramer, F.; Heßler, N.; Hornung, M.; Schmauder, H.-P.; Marsch, S. Nanocelluloses as Innovative Polymers in Research and Application. In *Polysaccharides Ii*; 2006; pp 49-96.
(7) Sirviö, J. A.; Honkaniemi, S.; Visanko, M.; Liimatainen, H. Composite Films of Poly(Vinyl Alcohol) and Bifunctional Cross-Linking Cellulose Nanocrystals. *ACS Appl. Mater. Interfaces* **2015,** *7* (35), 19691-19699, DOI: 10.1021/acsami.5b04879.
(8) Karim, Z.; Mathew, A. P.; Grahn, M.; Mouzon, J.; Oksman, K. Nanoporous Membranes with Cellulose Nanocrystals as Functional Entity in Chitosan: Removal of Dyes from Water. *Carbohydr. Polym.* **2014,** *112*, 668-676, DOI: https://doi.org/10.1016/j.carbpol.2014.06.048.
(9) Mautner, A.; Lee, K.-Y.; Tammelin, T.; Mathew, A. P.; Nedoma, A. J.; Li, K.; Bismarck, A. Cellulose Nanopapers as Tight Aqueous Ultra-Filtration Membranes. *React. Funct. Polym.* **2015,** *86*, 209-214, DOI: https://doi.org/10.1016/j.reactfunctpolym.2014.09.014.
(10) Quellmalz, A.; Mihranyan, A. Citric Acid Cross-Linked Nanocellulose-Based Paper for Size-Exclusion Nanofiltration. *ACS Biomater. Sci. Eng.* **2015,** *1* (4), 271-276, DOI: 10.1021/ab500161x.
(11) Karim, Z.; Claudpierre, S.; Grahn, M.; Oksman, K.; Mathew, A. P. Nanocellulose Based Functional Membranes for Water Cleaning: Tailoring of Mechanical Properties, Porosity and Metal Ion Capture. *J. Membr. Sci.* **2016,** *514*, 418-428, DOI: https://doi.org/10.1016/j.memsci.2016.05.018.
(12) Ferraz, N.; Leschinskaya, A.; Toomadj, F.; Fellström, B.; Strømme, M.; Mihranyan, A. Membrane Characterization and Solute Diffusion in Porous Composite Nanocellulose Membranes for Hemodialysis. *Cellulose* **2013,** *20* (6), 2959-2970, DOI: 10.1007/s10570-013-0045-x.
(13) Karim, Z.; Mathew, A. P.; Kokol, V.; Wei, J.; Grahn, M. High-Flux Affinity Membranes Based on Cellulose Nanocomposites for Removal of Heavy Metal Ions from Industrial Effluents. *RSC Adv.* **2016,** *6* (25), 20644-20653, DOI: 10.1039/C5RA27059F.
(14) Niazi, M. B. K.; Jahan, Z.; Berg, S. S.; Gregersen, Ø. W. Mechanical, Thermal and Swelling Properties of Phosphorylated Nanocellulose Fibrils/PVA Nanocomposite Membranes. *Carbohydr. Polym.* **2017,** *177*, 258-268, DOI: https://doi.org/10.1016/j.carbpol.2017.08.125.
(15) Zhang, X.-F.; Hou, T.; Chen, J.; Feng, Y.; Li, B.; Gu, X.; He, M.; Yao, J. Facilitated Transport of CO_2 through the Transparent and Flexible Cellulose Membrane Promoted by Fixed-Site Carrier. *ACS Appl. Mater. Interfaces* **2018,** *10* (29), 24930-24936, DOI: 10.1021/acsami.8b07309.
(16) Ansaloni, L.; Salas-Gay, J.; Ligi, S.; Baschetti, M. G. Nanocellulose-Based Membranes for CO_2 Capture. *J. Membr. Sci.* **2017,** *522*, 216-225, DOI: 10.1016/j.memsci.2016.09.024.
(17) Venturi, D.; Grupkovic, D.; Sisti, L.; Baschetti, M. G. Effect of Humidity and Nanocellulose Content on Polyvinylamine-Nanocellulose Hybrid Membranes for CO_2 Capture. *J. Membr. Sci.* **2018,** *548*, 263-274, DOI: https://doi.org/10.1016/j.memsci.2017.11.021.
(18) Venturia, D.; Ansalonib, L.; Baschettia, M. G. Nanocellulose Based Facilitated Transport Membranes for Co_2 Separation. *Chem. Eng. Trans.* **2016,** *47*.
(19) Hosakun, Y.; Halász, K.; Horváth, M.; Csóka, L.; Djoković, V. Atr-Ftir Study of the Interaction of CO_2 with Bacterial Cellulose-Based Membranes. *Chem. Eng. J.* **2017,** *324*, 83-92, DOI: https://doi.org/10.1016/j.cej.2017.05.029.
(20) Baker, R. W.; Low, B. T. Gas Separation Membrane Materials: A Perspective. *Macromolecules* **2014,** *47* (20), 6999-7013, DOI: 10.1021/ma501488s.
(21) Jahan, Z.; Niazi, M. B. K.; Hägg, M.-B.; Gregersen, Ø. W. Decoupling the Effect of Membrane Thickness and Cnc Concentration in PVA Based Nanocomposite Membranes for CO_2/CH_4 Separation. *Sep. Purif. Technol.* **2018,** *204*, 220-225, DOI: https://doi.org/10.1016/j.seppur.2018.04.076.
(22) Torstensen, J. Ø.; Helberg, R. M. L.; Deng, L.; Gregersen, Ø. W.; Syverud, K. PVA/Nanocellulose Nanocomposite Membranes for CO_2 Separation from Flue Gas. *Int. J. Greenhouse Gas Control* **2019,** *81*, 93-102, DOI: https://doi.org/10.1016/j.ijggc.2018.10.007.

(23) Dai, Z.; Ansaloni, L.; Deng, L. Recent Advances in Multi-Layer Composite Polymeric Membranes for CO_2 Separation: A Review. *Green Energy Environ.* **2016,** *1* (2), 102-128, DOI: https://doi.org/10.1016/j.gee.2016.08.001.
(24) Deng, L.; Hägg, M.-B. Fabrication and Evaluation of a Blend Facilitated Transport Membrane for CO_2/CH_4 Separation. *Ind. Eng. Chem. Res.* **2015,** *54* (44), 11139-11150, DOI: 10.1021/acs.iecr.5b02971.
(25) Saeed, M.; Deng, L. Carbon Nanotube Enhanced PVA-Mimic Enzyme Membrane for Post-Combustion CO_2 Capture. *Int. J. Greenhouse Gas Control* **2016,** *53*, 254-262, DOI: https://doi.org/10.1016/j.ijggc.2016.08.017.
(26) Dai, Z.; Ansaloni, L.; Deng, L. Precombustion Co_2 Capture in Polymeric Hollow Fiber Membrane Contactors Using Ionic Liquids: Porous Membrane Versus Nonporous Composite Membrane. *Ind. Eng. Chem. Res.* **2016,** *55* (20), 5983-5992, DOI: 10.1021/acs.iecr.6b01247.
(27) Rea, R.; Ligi, S.; Christian, M.; Morandi, V.; Giacinti Baschetti, M.; De Angelis, M. G. Permeability and Selectivity of Ppo/Graphene Composites as Mixed Matrix Membranes for CO_2 Capture and Gas Separation. *Polymers* **2018,** *10* (2), 129.
(28) Ansaloni, L.; Rennemo, R.; Knuutila, H. K.; Deng, L. Development of Membrane Contactors Using Volatile Amine-Based Absorbents for CO_2 Capture: Amine Permeation through the Membrane. *J. Membr. Sci.* **2017,** *537*, 272-282, DOI: https://doi.org/10.1016/j.memsci.2017.05.016.
(29) Dai, Z.; Ansaloni, L.; Gin, D. L.; Noble, R. D.; Deng, L. Facile Fabrication of CO_2 Separation Membranes by Cross-Linking of Poly(Ethylene Glycol) Diglycidyl Ether with a Diamine and a Polyamine-Based Ionic Liquid. *J. Membr. Sci.* **2017,** *523*, 551-560, DOI: https://doi.org/10.1016/j.memsci.2016.10.026.
(30) Dufresne, A. Cellulose Nanomaterial Reinforced Polymer Nanocomposites. *Curr. Opin. Colloid Interface Sci.* **2017,** *29*, 1-8.
(31) Hamid, S. B. A.; Zain, S. K.; Das, R.; Centi, G. Synergic Effect of Tungstophosphoric Acid and Sonication for Rapid Synthesis of Crystalline Nanocellulose. *Carbohydr. Polym.* **2016,** *138*, 349-355, DOI: https://doi.org/10.1016/j.carbpol.2015.10.023.
(32) Xu, X.; Liu, F.; Jiang, L.; Zhu, J. Y.; Haagenson, D.; Wiesenborn, D. P. Cellulose Nanocrystals Vs. Cellulose Nanofibrils: A Comparative Study on Their Microstructures and Effects as Polymer Reinforcing Agents. *ACS Appl. Mater. Interfaces* **2013,** *5* (8), 2999-3009, DOI: 10.1021/am302624t.
(33) de Melo, E. M.; Clark, J. H.; Matharu, A. S. The Hy-Mass Concept: Hydrothermal Microwave Assisted Selective Scissoring of Cellulose for in Situ Production of (Meso)Porous Nanocellulose Fibrils and Crystals. *Green Chem.* **2017,** *19* (14), 3408-3417, DOI: 10.1039/C7GC01378G.
(34) Choo, K.; Ching, Y. C.; Chuah, C. H.; Julai, S.; Liou, N.-S. Preparation and Characterization of Polyvinyl Alcohol-Chitosan Composite Films Reinforced with Cellulose Nanofiber. *Materials* **2016,** *9* (8), 644, DOI: 10.3390/ma9080644.
(35) Saeed, M.; Rafiq, S.; Bergersen, L. H.; Deng, L. Tailoring of Water Swollen PVA Membrane for Hosting Carriers in CO_2 Facilitated Transport Membranes. *Sep. Purif. Technol.* **2017,** *179*, 550-560, DOI: https://doi.org/10.1016/j.seppur.2017.02.022.
(36) Peng, Y.; Gardner, D. J.; Han, Y.; Kiziltas, A.; Cai, Z.; Tshabalala, M. A. Influence of Drying Method on the Material Properties of Nanocellulose I: Thermostability and Crystallinity. *Cellulose* **2013,** *20* (5), 2379-2392, DOI: 10.1007/s10570-013-0019-z.
(37) Sofla, M. R. K.; Brown, R. J.; Tsuzuki, T.; Rainey, T. J. A Comparison of Cellulose Nanocrystals and Cellulose Nanofibres Extracted from Bagasse Using Acid and Ball Milling Methods. *Adv. Nat. Sci.: Nanosci. Nanotechnol.* **2016,** *7* (3), 035004.
(38) Rehman, N.; de Miranda, M. I. G.; Rosa, S. M. L.; Pimentel, D. M.; Nachtigall, S. M. B.; Bica, C. I. D. Cellulose and Nanocellulose from Maize Straw: An Insight on the Crystal Properties. *J. Polym. Environ.* **2014,** *22* (2), 252-259, DOI: 10.1007/s10924-013-0624-9.

(39) Holland, B. J.; Hay, J. N. The Thermal Degradation of Poly(Vinyl Acetate) Measured by Thermal Analysis–Fourier Transform Infrared Spectroscopy. *Polymer* **2002,** *43* (8), 2207-2211, DOI: https://doi.org/10.1016/S0032-3861(02)00038-1.
(40) Qi, H.; Cai, J.; Zhang, L.; Kuga, S. Properties of Films Composed of Cellulose Nanowhiskers and a Cellulose Matrix Regenerated from Alkali/Urea Solution. *Biomacromolecules* **2009,** *10* (6), 1597-1602, DOI: 10.1021/bm9001975.
(41) Garvey, C. J.; Parker, I. H.; Simon, G. P. On the Interpretation of X-Ray Diffraction Powder Patterns in Terms of the Nanostructure of Cellulose I Fibres. *Macromol. Chem. Phys.* **2005,** *206* (15), 1568-1575, DOI: 10.1002/macp.200500008.
(42) French, A. D.; Santiago Cintrón, M. Cellulose Polymorphy, Crystallite Size, and the Segal Crystallinity Index. *Cellulose* **2013,** *20* (1), 583-588, DOI: 10.1007/s10570-012-9833-y.
(43) Bansal, P.; Hall, M.; Realff, M. J.; Lee, J. H.; Bommarius, A. S. Multivariate Statistical Analysis of X-Ray Data from Cellulose: A New Method to Determine Degree of Crystallinity and Predict Hydrolysis Rates. *Bioresour. Technol.* **2010,** *101* (12), 4461-4471, DOI: https://doi.org/10.1016/j.biortech.2010.01.068.
(44) Segal, L.; Creely, J. J.; A.E. Martin, J.; Conrad, C. M. An Empirical Method for Estimating the Degree of Crystallinity of Native Cellulose Using the X-Ray Diffractometer. *Text. Res. J.* **1959,** *29* (10), 786-794, DOI: 10.1177/004051755902901003.
(45) Cho, M.-J.; Park, B.-D. Tensile and Thermal Properties of Nanocellulose-Reinforced Poly(Vinyl Alcohol) Nanocomposites. *J. Ind. Eng. Chem.* **2011,** *17* (1), 36-40, DOI: https://doi.org/10.1016/j.jiec.2010.10.006.
(46) Zidan, H. Structural Properties of CrF_3-and $MnCl_2$-Filled Poly (Vinyl Alcohol) Films. *J. Appl. Polym. Sci.* **2003,** *88* (5), 1115-1120.
(47) Anju, V.; Narayanankutty, S. K. Composites Part a Applied Science and Manufacturingpolyaniline Coated Cellulose Fiber/Polyvinyl Alcohol Composites with High Dielectric Permittivity and Low Percolation Threshold. *AIP Advances* **2016,** *6* (1), 015109.
(48) Deng, L.; Hägg, M.-B. Carbon Nanotube Reinforced PVAm/PVA Blend Fsc Nanocomposite Membrane for Co_2/Ch_4 Separation. *Int. J. Greenhouse Gas Control* **2014,** *26*, 127-134.
(49) Guo, X.; Wu, Y.; Xie, X. Water Vapor Sorption Properties of Cellulose Nanocrystals and Nanofibers Using Dynamic Vapor Sorption Apparatus. *Sci. Rep.* **2017,** *7* (1), 14207, DOI: 10.1038/s41598-017-14664-7.
(50) Torstensen, J. Ø.; Liu, M.; Jin, S.-A.; Deng, L.; Hawari, A. I.; Syverud, K.; Spontak, R. J.; Gregersen, Ø. W. Swelling and Free-Volume Characteristics of Tempo-Oxidized Cellulose Nanofibril Films. *Biomacromolecules* **2018,** *19* (3), 1016-1025, DOI: 10.1021/acs.biomac.7b01814.

TOC:

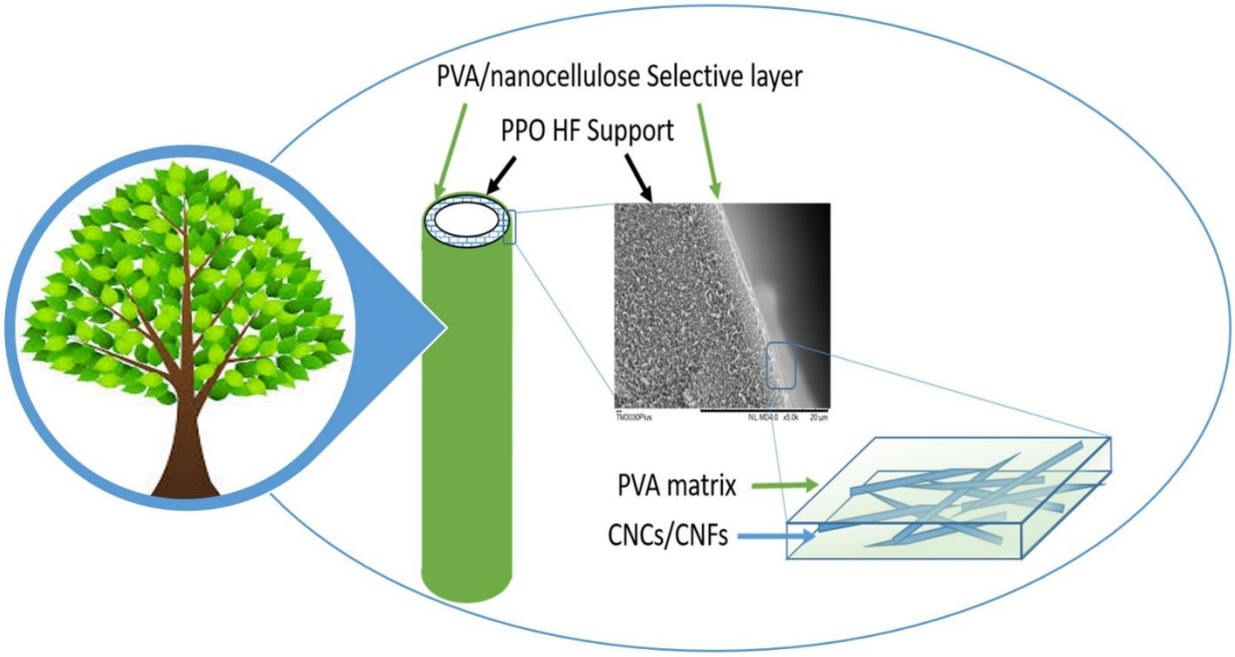
PVA/nanocellulose Selective layer
PPO HF Support
PVA matrix
CNCs/CNFs